Evaluating the Close-Companion Detection Capability of the Mount Wilson 100-inch Telescope for TESS Subgroup 3 Observations

Pat Boyce
Boyce Research Initiatives and Education Foundation
3540 Carleton St. San Diego, CA 92106
pat@boyce-astro.org

Fatemeh Fallahnejad
Boyce Research Initiatives and Education Foundation
fatemehfallah767@gmail.com

A. U. Kovic
Boyce Research Initiatives and Education Foundation
team.nonbionaries@gmail.com

Arturo Sorensen
Boyce Research Initiatives and Education Foundation
asorense@ucsd.edu

Joseph Soliz
Boyce Research Initiatives and Education Foundation
josephjsoliz@gmail.com

Thomas C. Smith
Dark Ridge Observatory
Tcsmith88354@gmail.com

Nathaniel Mackey
Boyce Research Initiatives and Education Foundation
nate@mackey.org

Geoff Stone
First Light Systems
geoff@first-light-systems.com

Abstract

This paper evaluates the ability to detect close companion stars using the 100-inch Hooker Telescope at Mount Wilson Observatory to demonstrate its capability to support the TESS Subgroup 3 (SG3) program. The SG3 program requires a system to be able to detect stellar companions with delta magnitudes of 5 or greater at separations of 0.5 arcsec or less with 5-sigma confidence. Our October 2025 observations were performed on targets using the 100-inch with the two-camera configuration suggested in Jackson et al. (SAS, 2025) with Sloan g′, r′, and i′ filters. We chose targets from the SG3 archive to compare the limits of this system's observation space with prior SG3 observations. We captured speckle interferometry data in Sloan g, r, and i, which is unique to SG3 observations, and reduced the data in four distinct tools for evaluation. Contrast curves developed as described in Howell et al. (2011) confirmed the system's ability to detect very close companions at the 5-sigma significance. Results suggest that this system can resolve close high delta magnitude companions in the SG3 requirement's space for primary targets that have companions above a limiting magnitude in good seeing conditions. The Hooker 100-inch Telescope can likely complement the capabilities of larger aperture observatories as a practical and student accessible observatory for a subset of SG3 targets.

1. Introduction

The detection and characterization of close stellar companions is an essential component of some modern observational programs, such as for exoplanet validation and follow-up studies. The Transiting Exoplanet Sky Survey's (TESS) goal is to identify exoplanet targets appropriate for allocating the precious James Webb Space Telescope's (JWST) observing time. The TESS's full qualification process is to filter from suspected candidates through five progressive levels of ground-based observing. The third follow-up stage, designated Subgroup 3 (SG3), uses high-resolution imaging to identify close stellar companions to candidate host stars. The light from a close companion can corrupt the measurement of the target's transit and thus its size and suitability for further observation.

Subgroup 3 observations require the ability to identify nearby stellar companions with magnitude differences (Δm) of up to 5 at angular separations of 0.5 arcseconds. These requirements are commonly addressed using large-aperture telescopes equipped with high-resolution imaging systems, often in the 4 to 8-meter class, using adaptive optics (AO) or speckle interferometry.

The availability of such facilities is limited, motivating the exploration of alternative platforms capable of contributing to SG3 objectives. The 100-inch Hooker Telescope at Mount Wilson Observatory (MWO) offers an opportunity to investigate whether a 2.5-meter-class telescope, equipped with modern speckle interferometry instrumentation, can achieve meaningful performance within the SG3 parameter space.

A speckle interferometry system for the Hooker Telescope has been previously developed and characterized (Ghent et al. 2025). That system was refined into a dual camera system for observations in 2025. The successful implementation of the system in 2025 had established a baseline operational performance that suggested the 100-inch could meet the SG3 requirements. The present study builds upon that foundation by focusing specifically on observational results relevant to SG3 requirements.

In this paper, we report on a series of observations of 13 target systems conducted to evaluate the practical limits of separation and contrast achievable with the Hooker Telescope. Attention is given to the system's ability to detect companions with Δm ≈ 5 at separations approaching 0.5 arcseconds, as exhibited in contrast curves. Targets were selected from previously observed SG3 targets for comparison. The results are intended to assess the role that this facility may play in supporting SG3 observations and to identify the conditions under which it can provide useful contributions. The results also inform future targeting decisions for close binary stars.

2. Instrumentation and Observational Setup

Observations were conducted at Mount Wilson Observatory using the 100-inch (2.54 m) Hooker Telescope on October 15 and 16, 2025.

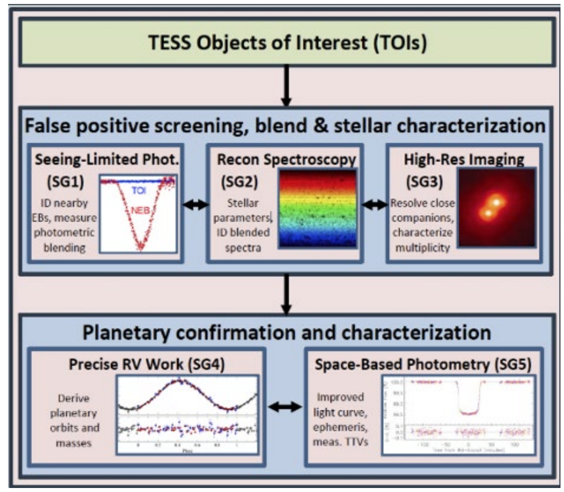

Figure 1: The TESS selection hierarchy: from the full TIC to TOIs, confirmed planets, and top exoplanet candidates.

2.1 Observing Site and Telescope

Mount Wilson Observatory (MWO), located in the San Gabriel Mountains northeast of Los Angeles, is historically recognized for stable atmospheric conditions favorable for high-angular-resolution observations. Typical seeing conditions historically range from approximately 0.7 to 2 arcsec.

The optical configuration for visual observations was unchanged but utilized a new instrument package (Section 2.2). Light from the north bent-Cassegrain port was redirected through a relay optical system into a 5-inch Explore Scientific refractor, which refocused the beam onto the detector focal plane. The configuration retained the Hooker Telescope's effective focal length of approximately 40.8 m (f/16). The optical configuration followed the general design previously developed for student speckle interferometry observations on the Hooker Telescope (Wasson et al. 2020).

Although Mount Wilson experiences moderate sky brightness associated with the Los Angeles metropolitan region, atmospheric stability and telescope thermal equilibrium are more significant factors affecting reconstructed speckle image quality. The observations reported here were obtained under suboptimal conditions beginning only a few hours after the end of a two-day storm at MWO. Due to these conditions, CHARA operations and seeing monitor were suspended that evening.

2.2 Bi-Camera Imaging System and Data Acquisition

A dual-camera ("bi-cam") system was designed and constructed by Lou Jackson (SAS, 2025) as a refinement to the speckle instrumentation described by Dale Ghent (SAS, 2025). The system incorporates a wide-field acquisition camera and a narrow-field science camera, enabling efficient target acquisition and high-resolution speckle imaging within a single integrated optical configuration.

The acquisition channel utilizes a ZWO ASI6200MM Pro camera (9576 × 6388 pixels) with an image scale of 0.0241 arcsec /pixel/and a measured position angle of 182.7°. This configuration provides a field of view of 3.85′ × 2.57′. The wide field enables reliable target identification, centering, and verification prior to high-resolution imaging.

The science channel employs a ZWO ASI585MM Pro camera (3840 × 2160 pixels) with an image scale of 0.0186 arcsec /pixel and a measured position angle of 189.8°. This camera, which has higher quantum efficiency in the near infrared, is well-suited for speckle interferometry. The resulting field of view is approximately 1.18′ × 0.67′, for capturing the full speckle pattern.

Switching between the acquisition and science channels is accomplished using a Baader Flip Mirror II driven by a ZWO EAF motor. The mirror is controlled through a second instance of NINA, where the flip mirror focuser at position 0 selects the acquisition camera, and the science camera is at 1800.

Observations were conducted by first acquiring and centering the target using the wide-field camera, followed by switching to the science camera to collect sequences of short-exposure frames in Sloan filters. The detector assembly, including cameras, filter integration, PC, and control electronics, is mounted on a stable platform attached to the optical transfer system. A photograph of the bi-camera instrument assembly is shown in Figure 2.

2.3 Observing Procedure

Targets were selected from TFOP SG3 objects spanning a range of separations, delta magnitudes, and apparent magnitudes. The telescope slit was positioned toward the south, and targets were acquired as they drifted into view. Restricting observations to targets below the zenith minimized telescope slewing time and improved observing efficiency during the limited observing interval.

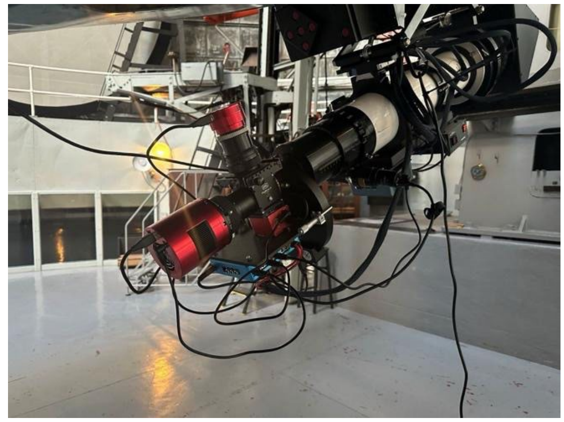

Figure 2: The bi-cam instrumentation secured to the Explore Scientific 5" refractor on the Hooker 100-inch Telescope.

Target selection and scheduling were supported by a program called Kepler, which displayed target positions against a sky background together with a simulated dome slit. Targets were selected dynamically as they entered the accessible observing region. Target coordinates were then relayed to the telescope operator, who manually centered the target using the wide-field acquisition camera. Following coarse centering, the narrow-field camera operator directed additional telescope adjustments to refine target positioning within the speckle imaging field.

Once centering was completed, the narrow-field operator optimized focus and initiated the automated NINA speckle imaging sequence which includes Sloan g′, r′, and i′. The operator first examined the speckle pattern using the suggested exposure time and then adjusted the exposure as necessary to achieve adequate image brightness. The ROI used for speckle imaging was 1024x1024 pixels, and exposure times ranged from 10 ms to 400 ms depending on target brightness and atmospheric conditions. One thousand frames were recorded for each target and corresponding reference star observation using Sloan g, r, and i filters.

Target observations were followed by reference star observations using the same acquisition procedure beginning with target selection through Kepler. Both target and reference image cubes were stored locally and simultaneously written to a server for later reduction and analysis.

Throughout the observing session, target observations were periodically suspended to observe widely separated known binary stars. These systems were used to determine plate scale and camera rotation through comparison with their known positions and proper motions.

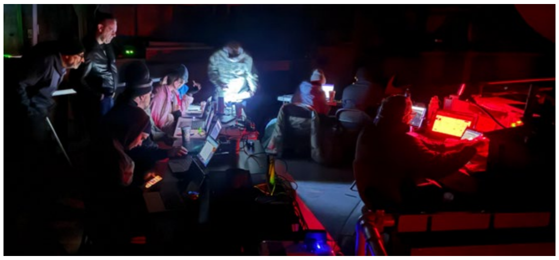

Figure 3: The observations team on October 15, 2025. The telescope operator station is on the right.

After approximately two hours of observing experience with the system and procedures, the observing team achieved an operational rate of approximately five target and reference star pairs per hour.

3. Observations

The targets we observed were derived from a list of 49 SG3 designations on October 15, 2025.

To minimize time delay, the dome slit was kept stationary throughout the night, as the telescope pointed south. Targets were chosen prioritizing the RA window as they passed over the slit and higher declinations for lower, more stable air mass.

In Table 1 (at end of the paper) we illustrate the total attempted observations. Of these some are noted to be removed from analysis due to inability to capture an appropriate reference star. In one case, we noticed that the reference star was actually a binary. In two other cases, a data problem resulted in missing reference star images in one or more filters.

We asked Dr. Rachel Matson of the USNO for targets of interest. She provided four of which we were able to observe two with IDs of MAT1 and MAT2. Observation information is outlined in Table 2 (at the end of the paper). Due to their RA they had to be observed on the night of October 16 as part of Mark Copper's investigation of Gaia 2 Parameter stars (G2P). The G2P project used IR Longpass and Luminance filters for the reference stars. For the STB reductions, the target Sloan g' observation was mapped to the Luminance reference filter; the Sloan r′ and i′ were mapped to the IR Longpass filter.

3.1 Seeing Conditions

Observations were obtained on 15 October 2025 between 21:00 and 01:00 PDT under post-frontal conditions following significant rainfall over the preceding two days. Skies cleared during the late afternoon, producing high atmospheric transparency; however, residual atmospheric instability associated with the cold air mass and boundary layer mixing resulted in degraded and variable seeing. CHARA did not operate, and no seeing monitor data is available for that night.

To properly assess the performance and uneven results, we needed to consider the seeing conditions for each target. Since we were lacking the essential seeing measures, Geoff Stone developed a program to assess the seeing quality by summing and separately stacking the reference star raw images that were captured for each target. The techniques employed are routine in the SOAR HRCam pipeline — Tokovinin 2018, PASP 130, 035002; and the Gemini Zorro/'Alopeke instruments — Scott et al. 2021. The reference-star observations are close in time, sky position, and filter to measure differential speckle motion for atmospheric r_0 (Sarazin & Roddier 1990) and contrast-vs-exposure-time for τ_0 (Karo & Schneiderman 1978). The program produces a Speckle Seeing Report in which RTN / hot pixels are either repaired or removed and provides the unregistered long-exposure FWHM alongside the SAA FWHM. Statistics such as drift and peak SNR and plots of the unregistered stack and the SAA stack over the image sequence are displayed. The report's Speckle Image Quality (SIQ) metric is the long-exposure FWHM for the "delivered seeing" at the focal plane. The SIQ for the reference star for each target was computed and is posted in Table 3 (at the end of the paper).

4. Data Reduction and Analysis Pipeline

Our data reduction pipeline is illustrated in Figure 4. We begin with the raw data which is 1000 short exposure images of both the target and reference star in each Sloan g′, r′, and i′ filter. Exposure times were chosen depending on the target's magnitude.

Each target and reference star were observed in pairs chronologically and therefore under similar seeing conditions. Reference stars were chosen for each target based on comparable brightness and closeness in RA and Dec. The images of both the target and reference stars were saved as .fit files and funneled into two different processing programs: Speckle Toolbox and SpeckleBSP GUI.

4.1 Calibration

We determined the plate scale and rotation angle of the camera by imaging known calibration

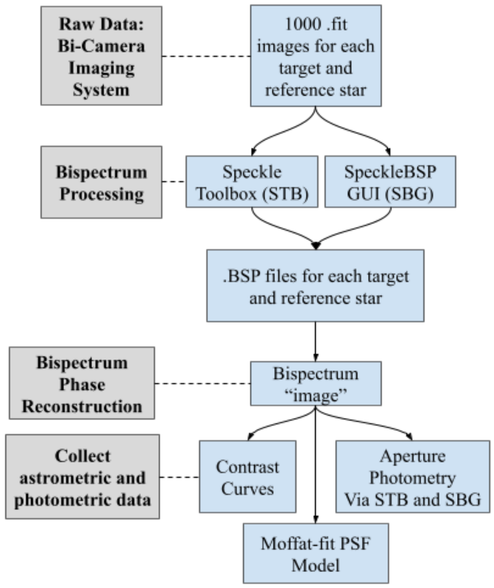

Figure 4. Illustration of Data Reduction Pipeline

doubles and comparing our observed astrometric data with separations measured in Gaia Data Release 3 (DR3). We corrected the DR3 RA and Dec of each star from the reference epoch J2016.0 to J2025.8 by way of computing their expected movement from their known proper motion vectors.

Calibration was performed on two nights: October 15 and 17. We imaged three calibration doubles on October 15 and two calibration doubles on October 17. For data collected on October 16, we took the mean between the two nights' values. The computed calibration values are displayed in Table 4.

4.2 Bispectrum Processing and Phase Reconstruction

The raw FITS image cubes are processed with both Speckle Toolbox and SpeckleBSP GUI. These processes both output .bsp1 files, which contain the Fourier-transformed speckle data. These files serve as the input for phase-reconstruction to determine if a companion can be detected. The files were imported into another feature of Speckle Toolbox: Bispectrum Phase Reconstruction, where astrometric analysis is performed. For further astrometric, photometric, and contrast-curve analysis, we exported the reconstructed images into other programs outlined in the pipeline.

	October 15, 2025	October 16, 2025	October 17, 2025
Camera Rotation Angle (°)	4.36	4.33	4.30
St Dev	0.25		0.14
Arcseconds/pix	0.01973	0.01921	0.01868
St Dev	0.00266		0.00003

Table 4: Calibration measurements by night

4.3 Collect astrometric and photometric data

The reconstructed FITS images were analyzed to extract astrometric and photometric measurements of detected companions. Quantities included the angular separation (ρ) and delta magnitude (Δm) between the target and its companion for each filter.

Astrometric measurements were obtained through the image scale calculated by the calibration binaries described in section 4.1. Gaussian and Moffat profile fitting routines were used to determine the centroids of each star and their relative fluxes for photometry analysis.

The reconstructed images were then used to generate contrast-curves to quantify the detection sensitivity with respect to the angular separation between target and companion.

5. Software

5.1 Speckle Toolbox (v10.03)

Speckle Toolbox (STB) is a speckle interferometry reduction tool used several times throughout our pipeline. STB reads the bispectrum products generated during processing and reconstructs images of stars with very small separations (Harshaw, R. et al. 2017). An example of its use can be seen in Figure 5. The software also provides tools for performing astrometry and

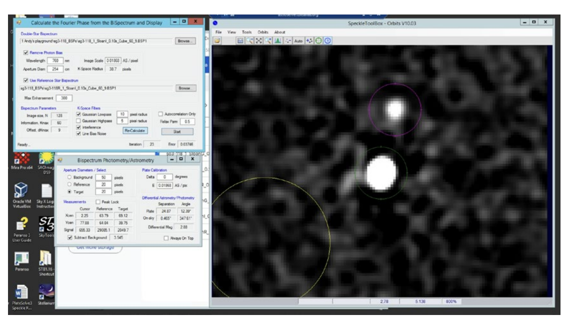

Figure 5. Speckle Toolbox display showing the reconstructed bispectrum "image" of SG118 in the Sloan i' filter.

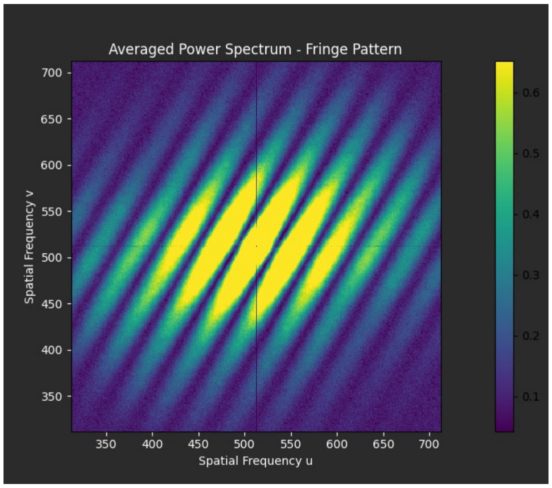

Figure 6. Averaged Power Spectrum – Fringe Pattern for Target SG3 captured with the Sloan r′ filter.

photometry. The resulting reconstructed FITS images served as the basis for all final astrometric and photometric analysis presented in this work.

5.2 SpeckleBSP GUI

During the speckle image acquisition, frames were processed in near-real-time using SpeckleBSP (v4.1.0), a Windows application developed by Geoff Stone for bispectrum processing of speckle interferometry data.

The application's Fringe Pattern tool computed an averaged Fourier power spectrum across the accumulated FITS frames in the active observation directory and, on demand or at a user-specified periodic interval, refreshed three diagnostic displays: a fringe (power-spectrum) image revealing the characteristic Young's-fringe pattern of a binary, an autocorrelation image in which a companion appears as symmetric side-lobes about the central peak, and a one-dimensional ADU slice taken along the detected binary-separation axis through the central autocorrelation peak (see Figure 6).

Automatic peak detection marked candidate companions and reported separation and position angle, while controls for log/asinh stretch, central-peak suppression, and contrast allowed weak companions to be teased out of the noise. These at-the-telescope diagnostics let the observer confirm the presence of a companion mid-run and, with practice, adjust acquisition parameters such as exposure time or frame count to improve fringe contrast before moving to the next target.

For final reduction, the same application produced a .bsp1 bispectrum file — with optional dark-frame subtraction, RTN-pixel correction, and reference-star normalization applied during the averaging — which was then fed to Speckle Tool Box for bispectrum phase reconstruction. These largely automated reductions were compared with manually developed bispectrum reconstructions and are displayed in Section 6.

5.3 Contrast Curve Generator (v1.4)

To quantify the detection sensitivity of each reconstructed image, the phase-recovered frames produced by STB were analyzed with Contrast Curve Generator, a companion tool also developed by Geoff Stone. The program reads the reconstructed FITS image, locates the primary on the brightest pixel, and measures the point-spread-function FWHM from a radial profile to characterize the delivered image quality. It then steps outward in concentric one-pixel-wide annuli (with a configurable analysis range) and, in each annulus, identifies every local maximum and minimum. The detection threshold follows the construction of Horch et al. (2011) and Howell et al. (2011) — now standard in the speckle-imaging literature (e.g., Horch et al. 2017; Scott et al. 2021; Howell & Furlan 2022; Howell et al. 2024) — but uses the median and MAD-derived σ in place of the mean and standard deviation for robustness against the bright reconstruction sidelobes that commonly contaminate phase-recovered speckle frames. Per-annulus statistics are computed on halo-subtracted local extrema, and the resulting curve is lightly smoothed with a Gaussian kernel before conversion from linear flux to a Δ magnitude relative to the primary's peak.

The generator produced the example contrast curve (Figure 7), plotted on dual axes in both arcseconds and pixels, with all detected local maxima (open squares) and minima (filled dots) overlaid on the 5σ detection-limit curve. Significant detections — local maxima rising above the 5σ threshold — are flagged automatically on the plot, providing an objective check on the companions identified in real time at the telescope by SpeckleBSP. Thumbnails of all contrast curves are shown in Appendix I.

5.4 Moffat Profile Fitting

Speckle Toolbox and Speckle BSP GUI are programs that utilize a gaussian fit to determine centroids of stars and measure flux. Reconstructed images using Speckle Toolbox were also analyzed using a Moffat profile fitting. A Moffat profile may be preferred to a gaussian profile due to its ability to

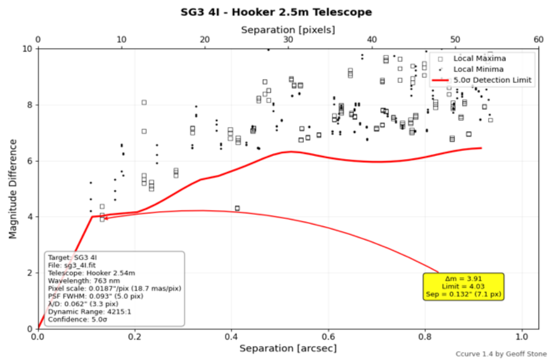

Figure 7. Generated contrast curve for ID SG4 captured with the Sloan i′ filter.

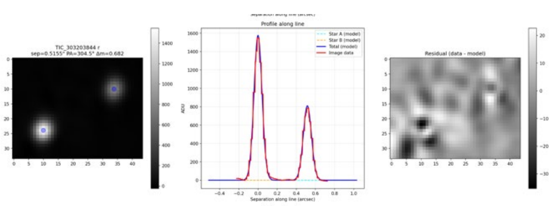

Figure 8. Moffat fitting profile output image for ID SG3 in the Sloan r′ filter.

match the atmospheric turbulence prediction of the PSF (Trujillo et al. 2001).

We used a program developed by Frank Suits to perform the Moffat fit on each target. The output of this program is a set of three images. Figure 8 shows an example of a successful detection. The first image is the reconstructed speckle image. The two bright spots are the primary and secondary components of the binary. Separation, position angle, and delta magnitude are recorded here. The second image is an intensity profile along the axis that cuts through the centroids of the components. In the successful detection, the curve for observed image data and the curve representing the sum of the Moffat models for A and B are very close, indicating a good fit. The third image is a residual image constructed by subtracting the model (middle image) from the reconstructed image (left image). The light regions indicate where the model underestimates the data and the dark regions indicate where the model overestimates the data.

Moffat fittings for all successful companion detections are in Appendix II.

6. Results

The results can be found in Table 5 (at the end of the paper). As noted in Section 3, some attempted targets are removed from analysis are therefore not present in this table. Companion non-detection is noted for targets whose companions could not be resolved. Separation and delta magnitude are recorded for each target for each filter for each processing method: STB, STB GUI, and Moffat. STB GUI does not record delta magnitude.

4 of 10 of our targets were complete non-detections. That is, no companion was detected through any methods outlined in the data reduction pipeline. 4 of 10 of our targets were partial non-detections where a companion was detected in one or more filters, but not all. We noted that 3 of the 4 partial non-detections, were non-detections in the Sloan g′ filter. 1 of these partial non-detections was in the Sloan i′ filter.

In our results table we have a comparison of three methods described previously in this section: Speckle Toolbox, STB GUI, and Moffat Profile Fitting. All three methods show general agreement, with the exception of SG119. Speckle Toolbox and Contrast Curve data is compared in Table 3. STB GUI did not detect companions for 3 of 10 of our targets.

7. Comparison with SG3 Observatories

Targets were selected from the completed SG3 observations in TESS ExoFOP database as a means to compare the 100-inch performance with the current observatories in the program (Table 3)

A wide range of targets were selected spanning separations, magnitudes and delta magnitudes to try to define an envelope of target parameters suitable for MWO 100-inch observations for SG3. By necessity several targets would extend beyond the envelope of observability to define the observable boundaries.

Table 6 (at the end of the paper) compares the reported ExoFOP parameters for the targets by Observatory for comparison to our results on the MWO 100-inch the nights of October 15 and 16, 2025. The MWO observation parameters are listed in the center with the measurements using STB and Contrast Curves to the right. Notes about the results for each target are listed on the far right.

There are wide gaps in the targets observed. Despite having a large target list, we were only able to attempt 13 observations in the four hours' time. There were no observed targets with a companion magnitude between 13 (MAT2) and 14.9 (SG7). An edge to the observable envelope would seem to fall in this region and needs to be explored. There was only one target (MAT1) with a delta magnitude over 5 and it was too wide for our planned measurements and needs to be reduced again.

Most prior observations have not been made in broadband filters like the Sloan, g′, r′, and i′. Results are very dependent upon the filter band and that makes direct comparisons difficult.

8. Discussion

Our observations suggest the possibility of SG3-level performance under favorable conditions, but do not yet conclusively demonstrate it. The targets observed did not directly test for a companion that was Δ mag ≥ 5 at ≤0.5″, the SG3 requirement. The practical detection limit observed in this study was dominated less by telescope the diffraction limit and more by atmospheric image quality, companion magnitude and the speckle data reduction uncertainties. The observations suggest that successful identification of close companions is more likely when SIQ conditions are below approximately 2.

There are limited data from this initial test. We were able to attempt to observe 13 of our 49 targets on our list. During the manual observing process a software error discovered early in the four-hour run limited the early production while corrections were made. The outcomes tabulated in Table 7. Each of the failure modes are discussed below and can be addressed in future observations.

Table 7 Observational results were strongly impacted by seeing as estimated by SIQ. The targets in Table 7 are also plotted with respect to their separation and secondary magnitude (Figure 9 at the end of the paper). From this figure, we notice the ability to detect a companion falls off with secondary stars dimmer than 13th magnitude.

Future tests will have a target list narrowed to test the envelope of observability to confirm Gaia SG3 level performance. Targets will be selected with known companions brighter than 15th magnitude, delta magnitudes between 3 and 7 and separations in the 0.3” to 0.7” range. This will test the envelope more precisely and not waste observation time on less informative targets.

More successful results can be expected with a higher cadence of observing with improvements in procedures and software. The NINA software is designed for automated observing which is not possible with the 100-inch. Thus, the software workflow must be modified for partially manual operation with the 100-inch telescope. The functions need to be improved for the manual operations. Areas for improvement include an improved focusing process, easier handoffs between functions, and more reliable data management. Real time assessment of observations by viewing fringes and exposure levels may also increase the reliability of observations. A real-time measure of SIQ and match with the new CHARA seeing monitor may improve target selection as well. The next goal should be a minimum of 5 targets and 5 references per hour with a 90+% success rate.

For the successful targets, the four different data reduction techniques had generally consistent results. These have not been tested with the same observations in the past. Separation values had less scatter than delta magnitudes. The contrast curves had a consistently higher delta magnitude than the STB reductions. Systemic biases or differences in sensitivities by tool should be identified. Possible false-positive detections near the sensitivity threshold require additional investigation. These disparities need to be evaluated and understood before the next observations. Additional evaluation of autocorrelation peaks and fringe visibility may improve discrimination between marginal detections and reduction artifacts. In addition to post observation analysis, the resolution of these may affect how real time assessments are performed and will affect the final data reduction.

The SG3 observatories have observed in narrow band filters which limit photometric analysis. Our three-color measurements from the 100-inch are unique for SG3 observations and enable more complete photometric analysis. Promising work is underway by an investigator on another project that would enable stellar classification for both stars from Sloan g′, r′, and i′ data such as reported here.

Total target list for selection during the 4 hours	**49**
Results	
Failed – lack of reference star due to procedural or software errors -	3
Failed – faint companion (<15 mag) and poor seeing (SIQ > 2.4)	3
Failed – false positive; low signal (possible under exposure) – need review	2
Failed – separation too small (0.118”) for poor seeing (SIQ 2.7)	1
Successful – SG3, SG4, SG118, and MAT 2	4

Table 7. Observational results for attempted observations.

9. Conclusion

The present study has been limited by a small sample size, uneven target coverage, poor seeing, incomplete coverage of the SG3 parameters, and a lack of seeing monitor data. No targets in the present dataset directly sampled the full SG3 requirement space of Δ m ≥ 5 at separations ≤0.5″.

Despite these limitations the Hooker 100-inch telescope appears capable of meaningful SG3 support for a subset of targets, but operational performance is limited more by atmospheric image quality, companion magnitude, and speckle data reduction uncertainties than by aperture diffraction limits. For future analysis, data has been gathered in three wide-band scientific filters and four reduction techniques. Results are sufficiently encouraging to undertake future observations to clarify its ability to support the TESS SG3 program.

In addition to its scientific potential, the MWO's Hooker Telescope TESS SG3 speckle program provides a valuable platform for student training in high-resolution astronomical instrumentation, observing operations, and data reduction. Such programs may help expand access to hands-on research experiences at a time when opportunities for undergraduate observational astronomy opportunities are increasingly limited.

10. Acknowledgements

This project was a true team effort with many contributors. The observations could not have been performed without Lou Jackson's design and construction of the bi-cam. Alexander Beltzer-Sweeney maintained the night's invaluable observation log. Mark Copper is acknowledged for assistance with target lists and observations of two (MAT) targets on October 16th. We followed Rick Wasson's calibration technique and he provided observation data for the night of October 17. Frank Suits developed the program to perform a Moffat fit analysis on our targets. Nick Hardy provided the NINA speckle plugin and assistance during the observing nights. Leon Bewersdorff operated the narrow-field camera and NINA software for data acquisition. Tom Meneghini operated the 100-inch Hooker Telescope during the observing sessions. Dave Rowe is acknowledged for the Kepler application, Plate Solve support, and the Speckle Toolbox. The authors also acknowledge the Boyce Research Initiatives and Education Foundation for funding support.

11. References

Ghent, D. et al, "Speckle Interferometry Camera Checkout on the 100-Inch Telescope at Mount Wilson Observatory" (2025), Proceedings for the 44th Annual Symposium on Telescope Science, 2025 June 19-21

Genet, R., & D. Rowe, T. Meneghini, R. Buchheim,R. Estrada, C. Estrada, P. Boyce, G. Boyce, J. Ridgely,N. Smidth, R Harshaw, and J. Kenney. 2016. Mt.Wilson 100-inch Speckle Interferometry Engineering Checkout. Journal of Double Star Observations, 12,263.

Hardy, N., L. Bewersdorff, D. Rowe, R. Genet, R.Wasson, J. Armstrong, S. Dixon, M. Harris, T. Smith,R. Freed, P. McCudden, S. Rajkumar, M. Davis, C Giavarini, R. Snyder, R. Wolly, M. Calvin, S. Cotton, & M Rabin. 2023. Automated Speckle Interferometry of Known Binaries: With WDS 12274-2843 B228 as an Example. Journal of Double Star Observations, 19, 106.

Harshaw, R., D. Rowe, & R. Genet. 2017. The Speckle Toolbox: A Powerful Data Reduction Tool for CCD Astrometry. Journal of Double Star Observations, 13, 52.

Horch, E. P., Casetti-Dinescu, D. I., Camarata, M. A., et al., "Observations of Binary Stars with the Differential Speckle Survey Instrument. VII. Measures from 2010 September to 2012 February at the WIYN Telescope." (2017). AJ, 153, 212.

Horch, E. P., Gomez, S. C., Sherry, W. H., Howell, S. B., Ciardi, D. R., Anderson, L. M., & van Altena, W. F., "OBSERVATIONS OF BINARY STARS WITH THE DIFFERENTIAL SPECKLE SURVEY INSTRUMENT. II. HIPPARCOS STARS OBSERVED IN 2010 JANUARY AND JUNE." (2011). AJ, 141, 45.

Horch, E. P., Veillette, D. R., Baena Gallé, R., et al., "Observations of Binary Stars with the Differential Speckle Survey Instrument." (2009). AJ 137, 5057.

Howell, S. B., et al. 2025, arXiv:2503.10765.

Howell, S. B., Everett, M. E., Sherry, W., Horch, E., & Ciardi, D. R., "SPECKLE CAMERA OBSERVATIONS FOR THE NASA KEPLER MISSION FOLLOW-UP PROGRAM." (2011). AJ, 142, 19.

Howell, S. B., & Furlan, E., "Speckle Interferometric Observations With the Gemini 8-m Telescopes: Signal-to-Noise Calculations and Observational Results." (2022). Frontiers in Astronomy and Space Sciences 9, 871163.

Howell, S. B., Martinez, A. O., Hope, D. A., et al., "High-contrast, High-angular-resolution Optical Speckle Imaging: Uncovering Hidden Stellar Companions." (2024). AJ 167, 258.

Jackson, L., et al, "A Custom Speckle Interferometry Camera System for the Hooker

Telescope” (2025), Proceedings for the 44th Annual Symposium on Telescope Science, 2025 June 19-21

Karo, D. P., & Schneiderman, A. M., "Speckle interferometry with finite-bandwidth light: a theoretical and experimental study." (1978). J. Opt. Soc. Am. 68, 480.

Martinez, P., Kolb, J., Sarazin, M., & Tokovinin, A., "On the Difference between Seeing and Image Quality: When the Turbulence Outer Scale Enters the Game." (2010). ESO Messenger 141, 5.

Sarazin, M., & Roddier, F., "The ESO differential image motion monitor." (1990). A&A 227, 294.

Schneiderman, A. M., & Karo, D. P., "Speckle interferometry of stellar sources at 4880 Å." (1978). J. Opt. Soc. Am. 68, 348.

Scott, N. J., Howell, S. B., Gnilka, C. L., et al., "Twin High-Resolution, High-Speed Imagers for the Gemini Telescopes: Instrument Description and Science Verification Results." (2021). Frontiers in Astronomy and Space Sciences 8, 138.

Tokovinin, A., "From Differential Image Motion to Seeing." (2002). PASP 114, 1156.

Tokovinin, A., "Ten Years of Speckle Interferometry at SOAR." (2018). PASP 130, 035002.

Tokovinin, A., Mason, B. D., Hartkopf, W. I., Mendez, R. A., & Horch, E. P., "Speckle Interferometry at SOAR in 2016 and 2017." (2018). AJ 155, 235.

Tokovinin, A., Mason, B. D., Mendez, R. A., Horch, E. P., & Briceño, C., "Speckle Interferometry at SOAR in 2018." (2019). AJ 158, 48.

Tokovinin, A. 2024, arXiv:2408.12384.

Suits, F. 2025, SpeckleCap, Melbourne, Australia. https://www.smallstarspot.com/specklecap

Trujillo, Aguerri, Cepa, Gutiérrez, “The effects of seeing on Sérsic profiles – II. The Moffat PSF.” (2001). Monthly Notices of the Royal Astronomical Society 977, 985.

Wasson, R., et al., “A New Opportunity for Speckle Interferometry on the Mount Wilson 100-inch Telescope.” (2020). Journal of Double Star Observations, Vol. 16 No. 2 April 1, 2020.

(Tables and Appendix on following pages.)

Target	TESS Input Catalog ID	Sloan Filter	Exposure (ms)	Reference	Exposure (ms)	Seeing	Note
SG01	TIC_83958546	g′	40	binary			Da
		r′	60				
		i′	120				
SG03	TIC_303203844	g′	20	SS119186	20	1.78	A
		r′	′30		30		
		i′	60		50		
SG04	TIC_80474910	g′	20	SS77174	40	1.6	A
		r′	30		50		
		i′	60		100		
SG07	TIC_53875855	g′	50	SS100794	40	2.85	C
		r′	70		50		
		i′	140		100		
SG08	TIC_414922696	g′	110	SS124207	40	2.39	C
		r′	150		50		
		i′	300		100		
SG11	TIC_257922326	g′	80	SS61829		1.82	A, C
		r′	120		50		
		i′	240		100		
SG111	TIC_17865622	g′	30	data problem			Db
		r′	40				
		i′	80				
SG118	TIC_115771549	g′	40	SS278957	40	5.16	A
		r′	50		50		
		i′	100		100		
SG119	TIC_379660147	g′	10	SS95140	40	2.5	B
		r′	10		50		
		i′	20		100		
SG122	TIC_67478724	g′	50	SS195530	40	2.72	C
		r′	70		50		
		i′	140		100		
SG123	TIC_2040472616	g′	140	data problem			Db
		r′	200				
		i′	400				

Table 1. SG3 Target Selection and Exposure Values Per Filter. The following codes are used to classify each attempted target: A — Detection; B — Elongation; C — Non-detection; D — Excluded from analysis. Lowercase annotations indicate the reason for exclusion: a — Binary reference star; b — Missing reference star.

ID	Target	Filter	Exposure (ms)	Reference	Filter	Exposure (ms)	Seeing (arcsec)	Note
MAT1	TESS Object of Interest 1634	g′	70	G2P1182R	IR Longpass, Luminance	40	2.20	C
		r′	100			60		
		i′	200			60		
MAT2	Washington Double Stars Catalog 04201+3180	g′	40	G2P1200R	IR Longpass, Luminance	40	2.24	C
		r′	50			60		A
		i′	100			60		

Table 2. Additional Double Star Target Selection and Exposure Values Per Filter. The following codes are used to classify each attempted target: A — Detection; C — Non-detection.

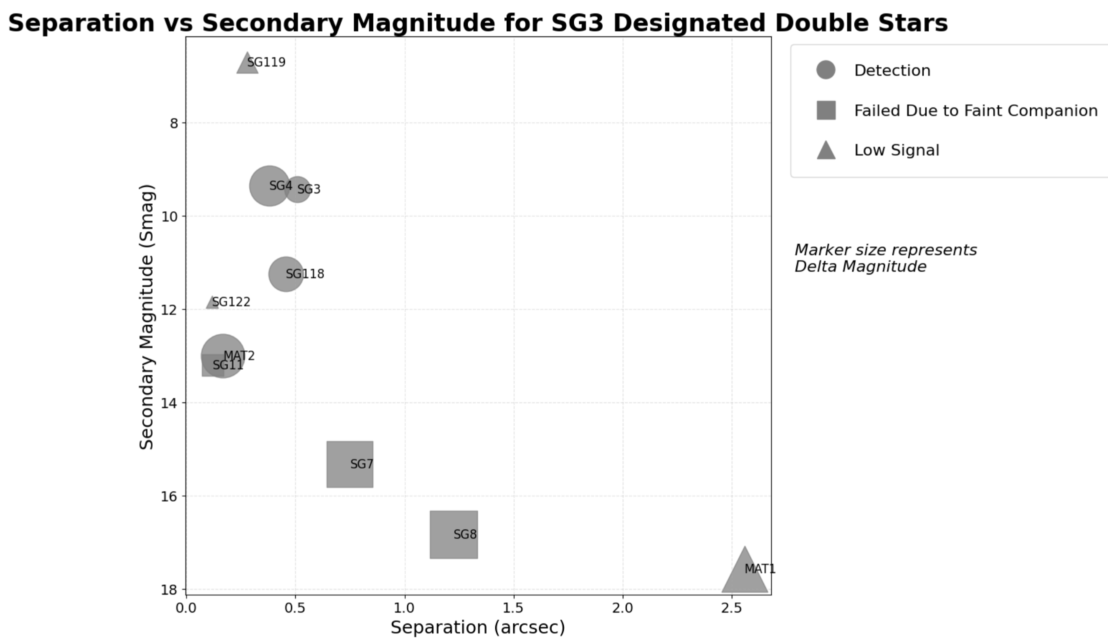

Figure 9. Separation vs Secondary Magnitude for each target for each filter. Delta magnitude is represented by marker size.

Table 3. Comparison Table

		DATA REPORTED In ExoFOP except as noted							MWO Observation			MWO RESULTS: STB Results		MWO RESULTS: Contrast Curves		Comments
Ref, ID	Target ID	Gaia mag	Observatory	Obs. Date	Filter	Sep. arcsec	Delta Mag	Sec. Mag.	Ref. SIQ	Exp. mas	Sloan Filter	Sep. arcsec	Delta Mag	Sep. arcsec	Delta Mag	
SG 3	TIC_303203844	8.02	NESSI@WIYN	01/27/23	562 (44) nm	0.51	1.42	9.51		20	g'	0.517	0.64	0.518	1.22	good result with good SIQ
			NESSI@WIYN	01/27/23	832 (40) nm	0.511	0.95	8.64	1.78	30	r'	0.516	0.57	0.519	0.74	
										60	I'	0.516	0.47	0.419	0.69	
SG 4	TIC_80474910	6.02	Gemini (8 m)	12/03/20	562 (54) nm	0.382	3.74	9.81		20	g'	0.406	3.74	0.393	4.81	large delta magnitude; good result with good SIQ
			Gemini (8 m)	12/03/20	832 (40) nm	0.381	3.34	9.19	1.6	30	r'	0.406	3.25	0.411	4.42	
										60	I'	0.403	3.09	4.1	4.1	
SG 7	TIC_53875855	10.8								70	g'	Companion Not Detected				faint secondary star; probably below 100" threshhold; uncertain
			SAI-2.5m	12/02/20	I	0.75	4.7	15.1	2.85	70	r'					
			Gemini (8 m)	12/03/20	832 (40) nm	0.75	4.48	14.9		140	I'					
SG 8	TIC_414922696									110	g'	Companion Not Detected				faint secondary star; probably below 100" threshhold; uncertain due to
									2.39	250	r'					
		12.34	NESSI@WIYN	10/28/21	832 (40) nm	1.225	4.5	16.4		300	I'					
SG 11	TIC_257922326	12.21	SOAR (4.1m)	01/04/23	879 (289) nm	0.121	0.4	12.2		80	r'	0.712	0.02	0.716	0.1	low signal caused false positives; need to review exposure
			SAI-2.5m	11/30/22	I	0.122	1± 0.1	12.8	1.82	120	i'	Companion Not Detected				
										240						
SG 118	TIC_115771549	8.76	Gemini (8 m)	06/26/21	562 (54) nm	0.457	2.5	11.37	5.16	40	g'	0.449	3.37	0.458	4.27	wide enough to overcome very poor SIQ; compare to SG3 and
			Gemini (8 m)	06/26/21	832 (40) nm	0.459	2.63	11		50	r'	0.455	2.89	0.462	3.8	
			Palomar (5m)	06/19/21	Brgamma	0.45	2.82	10.3		100	I'	0.461	2.88	0.458	3.98	
SG 119	TIC_379660147	5.87	Gemini (8 m)	09/17/21	562 (54) nm	0.279	1.04	6.78	2.5	10	g'	0.083	0.69	Companion Not Detected		elongation observed; exposure maybe too short; poor SIQ Moffat
			Gemini (8 m)	06/27/21	562 (54) nm	0.291	0.91	6.65		10	r'	0.085	0.73			
			Gemini (8 m)	06/27/21	620 (145) nm	0.292	1.15	6.44		20	I'	0.09	0.95			
			Gemini (8 m)	06/27/21	765 (148) nm	0.29	1.14	6.43								
			Gemini (8 m)	06/27/21	832 (40) nm	0.29	1.15	6.44								
SG 122	TIC_67478724	11.50	Palomar (5m)	06/30/23	Hcont	0.118	0.352	10.5		50	g'	Companion Not Detected				SIQ too high for 0.118" separation; needs longer exposure
									2.72	70	r'					
										140	I'					
MAT 1	TOI1634	12.19	Gemini (8 m)	10/23/21	562 (54) nm	2.557	4.36	17.58	2.41	70	g'	Companion Not Detected		0.747	1.27	false positive; very wide and faint secondary; redo reduction with
			Gemini (8 m)	10/23/21	832 (40) nm	2.561	6.76	18.06		100	r'			0.374	1.27	
			Gemini (8 m)	02/16/20	562 (54) nm	2.538	4.81	18.03	2.07	200	I'					
			Gemini (8 m)	02/16/20	832 (40) nm	2.535	6.1	18.3								
MAT 2	WDS 04201+3108	8.68	from WDS	2011	V?	0.168	3.93	13.0	2.2	40	g'	Companion Not Detected				good result when SIQ < 2; change in separation may be orbital
										50	r'	0.286	3.63	0.109	3.94	
									1.91	100	I'	0.291	2.98	0.283	3.28	

ID	TESS Input Catalog (TIC)	Filter	STB Separation	STB Delta Mag	STB GUI Separation	Moffat Separation	Moffat Delta Mag
SG03	TIC_303203844	g′	0.517	0.64	0.493	0.516	0.92
		r′	0.516	0.57	0.519	0.515	0.61
		i′	0.516	0.47	0.519	0.516	0.68
SG04	TIC_80474910	g′	0.406	3.74	Companion not detected	0.401	2.914
		r′	0.406	3.25	0.392	0.408	2.94
		i′	0.403	3.09	0.411	0.404	3.04
SG07	TIC_53875855	g′	Companion not detected				
		r′					
		i′					
SG08	TIC_414922696	g′	Companion not detected				
		r′					
		i′					
SG11	TIC_257922326	r′	0.712	0.02	Companion not detected	0.715	0.04
		i′	Companion not detected				
SG118	TIC_115771549	g′	0.449	3.37	0.422	0.461	3.139
		r′	0.455	2.89	0.461	0.457	2.776
		i′	0.461	2.88	0.439	0.461	2.834
SG119	TIC_379660147	g′	0.083	0.69	Companion not detected	0.106	1.9
		r′	0.085	0.73	0.938	0.098	2.21
		i′	0.09	0.95	0.921	0.099	2.62
SG122	TIC_67478724	g′	Companion not detected				
		r′					
		i′					
MAT1	TOI 1634	g′	Companion not detected				
		r′					
		i′					
MAT2	WDS 04201+3108	g′	Companion not detected				
		r′	0.286	3.63	Companion not detected	0.284	3.35
		i′	0.291	2.98	Companion not detected	0.289	2.97

Table 5. Comparison of speckle binary star measurements across reduction methods and filters.

Observatory	Location	Altitude (m)	Latitude / Longitude (°)	Apertu re (m)	Diffractio n Limit*	Nominal Seeing
WIYN Observatory/ NESSI	Kitt Peak, Arizona, USA	2090	32° N, 112° W	3.5	~0.04″	~0.7–1.0″
Gemini Observatory / ‘Alopeke	Mauna Kea, Hawai‘i, USA	4213	20° N, 155° W	8.1	~0.017″	~0.4–0.7″
Sternberg Astronomical Institute 2.5m Telescope	Caucasus Mountain Observatory, Russia	~2112	43° N, 42° E	2.5	~0.06″	~1.0–1.5″
SOAR Telescope	Cerro Pachón, Chile	2738	30° S, 71° W	4.1	~0.03″	~0.5–0.8″
Palomar Observatory	Palomar Mountain, California, USA	1712	33° N, 117° W	5.1	~0.025″	~1.0″
Mount Wilson Observatory / Hooker Telescope	Mount Wilson, California, USA	1742	34° N, 118° W	2.5	~0.05″	~1.0–1.5″

Table 6. SG3 observatories and the telescope in comparison to the Mount Wilson Observatory 100-inch Hooker Telescope

(continued on next page)

12. Appendix I – Contract Curve Thumbnails

SG03 / TIC_303203844	SG04 / TIC_80474910

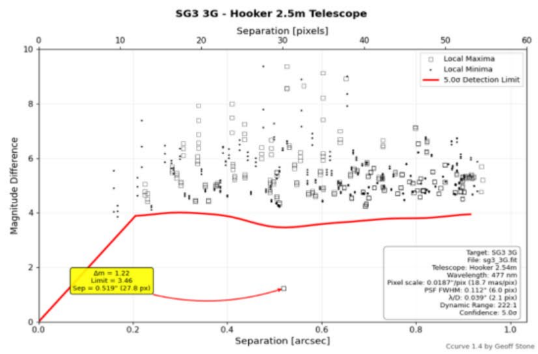

TIC_303203844, g' - Companion detected

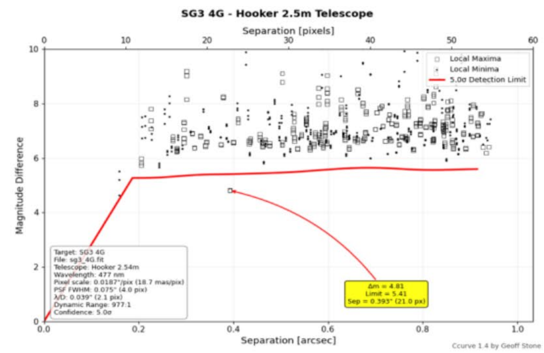

TIC_80474910, g' - Companion detected

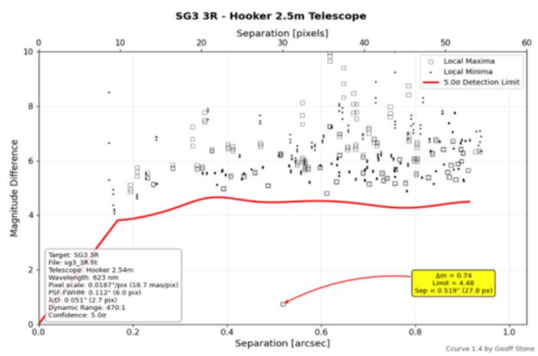

TIC_303203844, r' - Companion detected

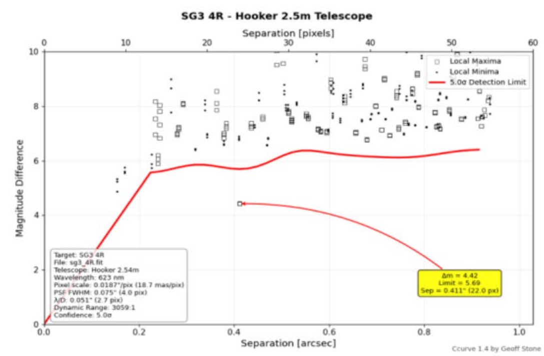

TIC_80474910, r' - Companion detected

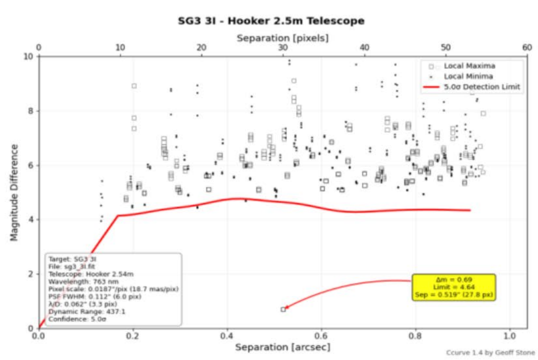

TIC_303203844, i' - Companion detected

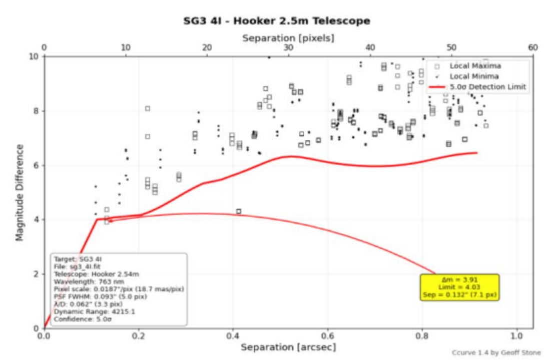

TIC_80474910, i' - Companion detected

SG118 / TIC_115771549	SG119 / TIC_379660147

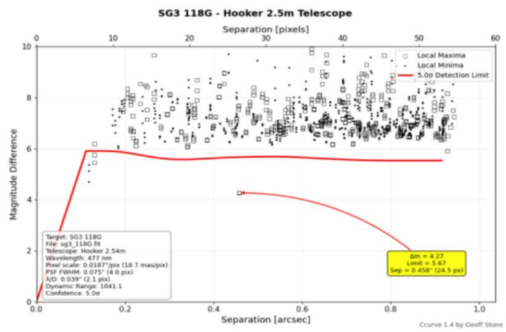

TIC_115771549, g' - Companion detected

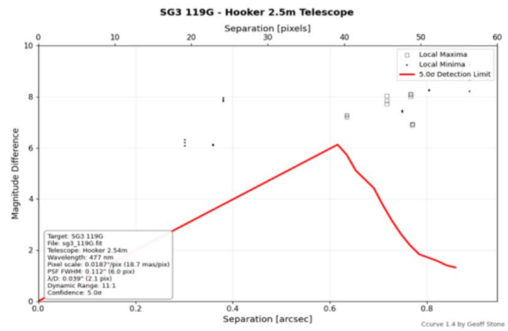

TIC_379660147, g' - Elongation / possible companion

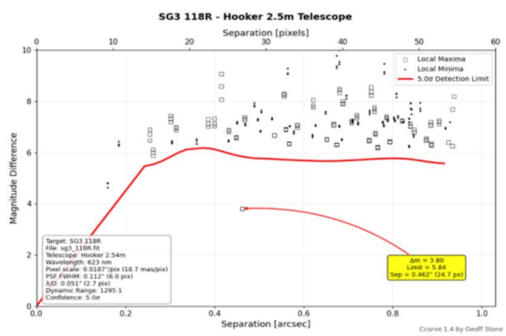

TIC_115771549, r' - Companion detected

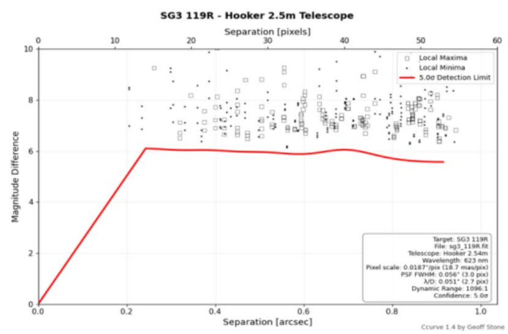

TIC_379660147, r' - Elongation / possible companion

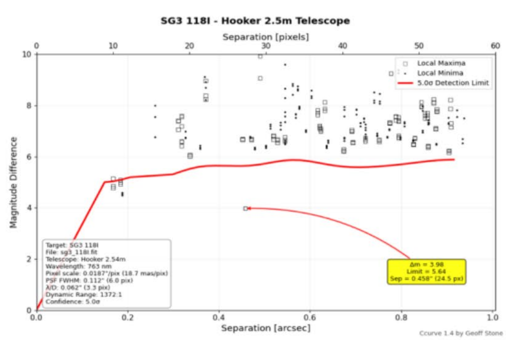

TIC_115771549, i' - Companion detected

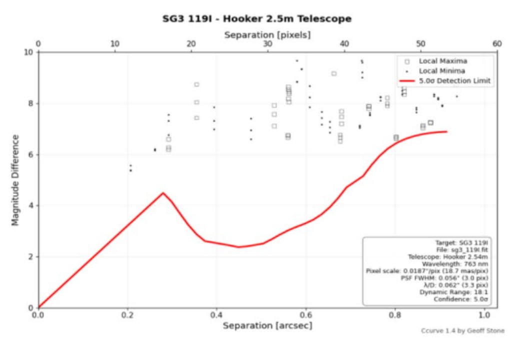

TIC_379660147, i' - Elongation / possible companion

MAT2 / WDS 04201+3108	SG11 / TIC_257922326

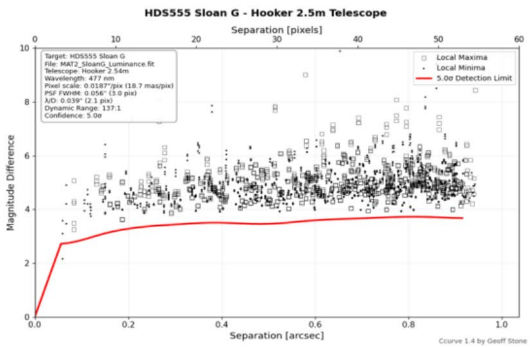

WDS 04201+3108, g' - Companion <u>not</u> detected

Not Captured

TIC_257922326, g' - filter not captured

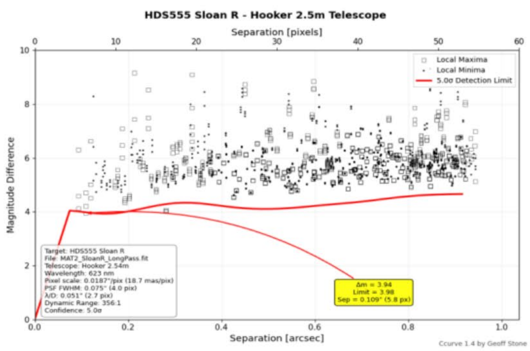

WDS 04201+3108, r' - Companion detected

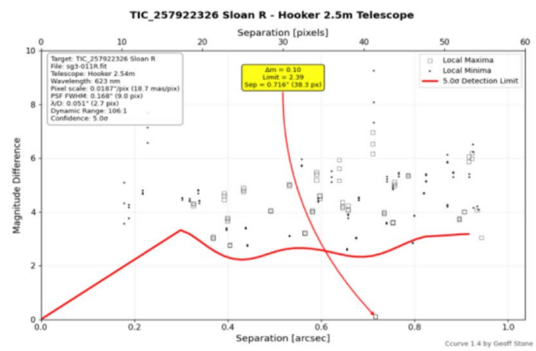

TIC_257922326, r' - Companion detected

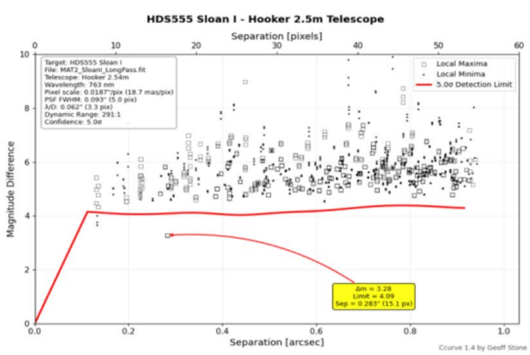

WDS 04201+3108, i' - Companion detected

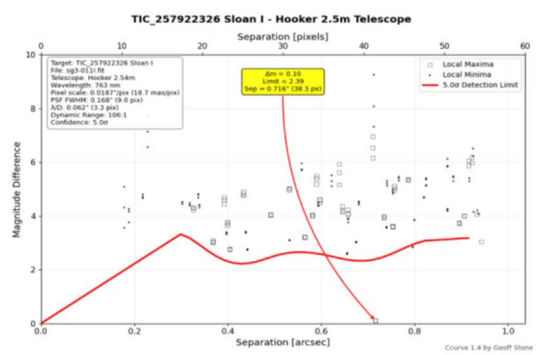

TIC_257922326, i' - Companion <u>not</u> detected

SG07 / TIC_53875855	SG08 / TIC_414922696

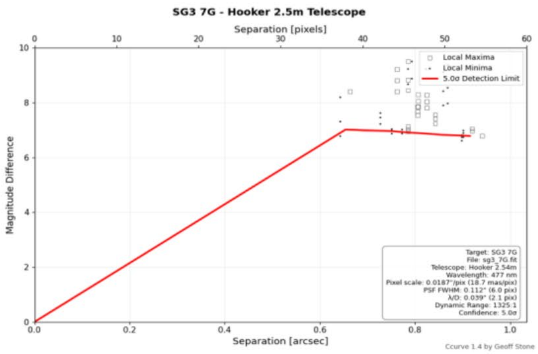

TIC_53875855, g' - Companion <u>not</u> detected

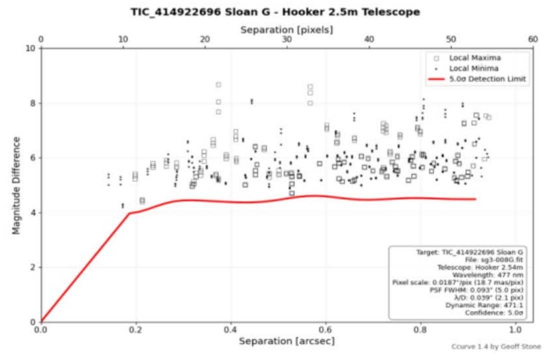

TIC_414922696, g' - Companion <u>not</u> detected

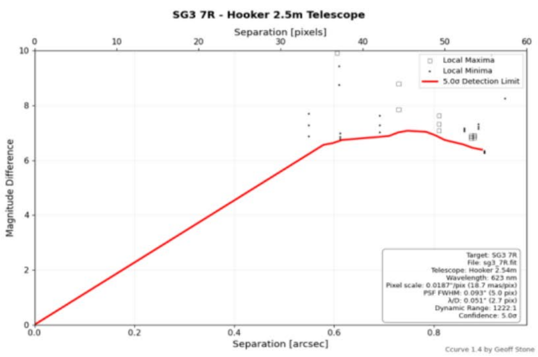

TIC_53875855, r' - Companion <u>not</u> detected

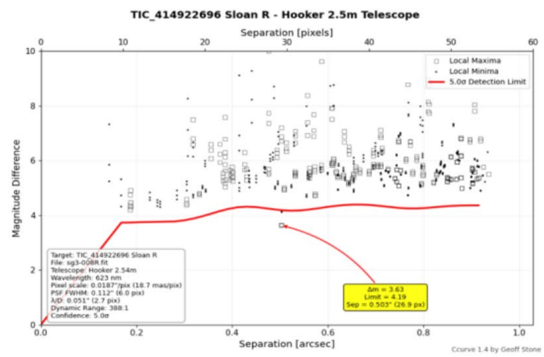

TIC_414922696, r' - Companion <u>not</u> detected

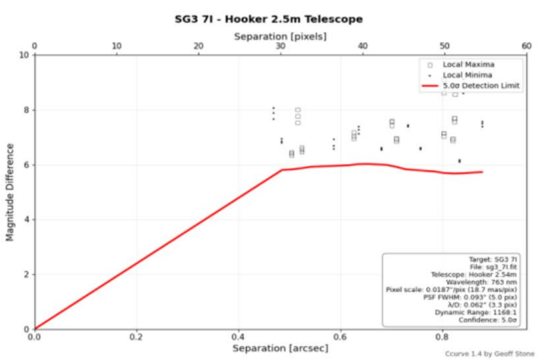

TIC_53875855, i' - Companion <u>not</u> detected

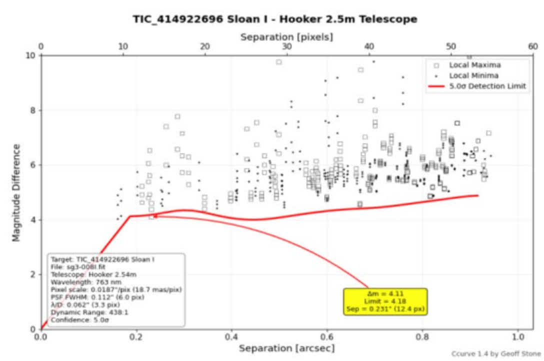

TIC_414922696, i' - Companion <u>not</u> detected

SG122 / TIC_67478724	MAT1 / TOI 1634

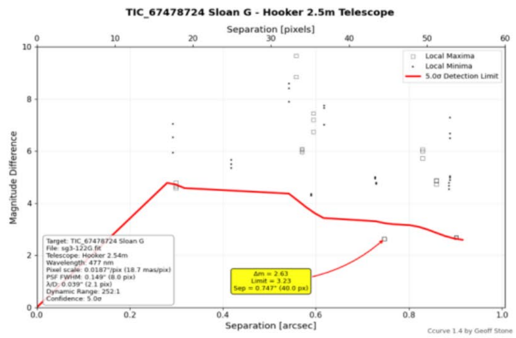

TIC_67478724, g' - Companion <u>not</u> detected

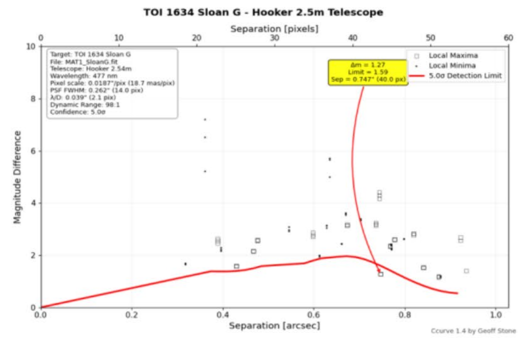

TOI 1634, g' - Companion <u>not</u> detected

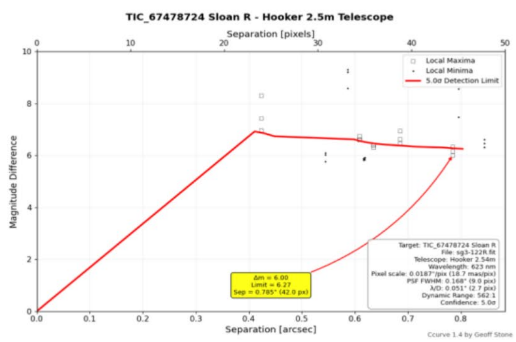

TIC_67478724, r' - Companion <u>not</u> detected

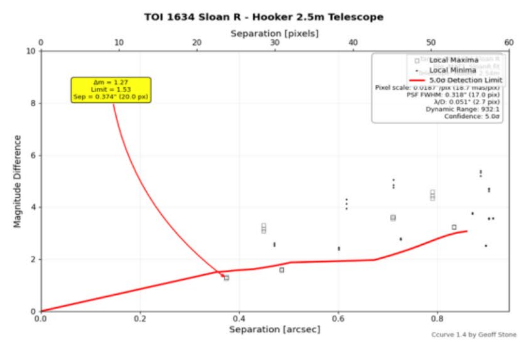

TOI 1634, r' - Companion <u>not</u> detected

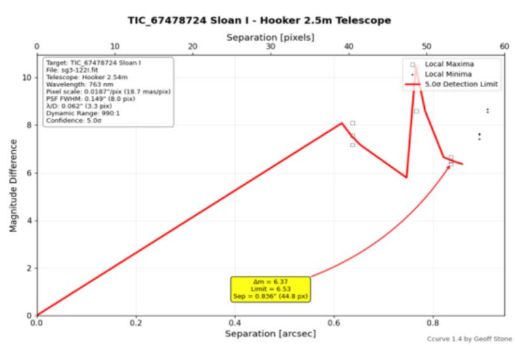

TIC_67478724, i' - Companion <u>not</u> detected

Unable to produce contrast curve

13. Appendix II. Moffat Fit Analysis

SG03 / TIC_303203844

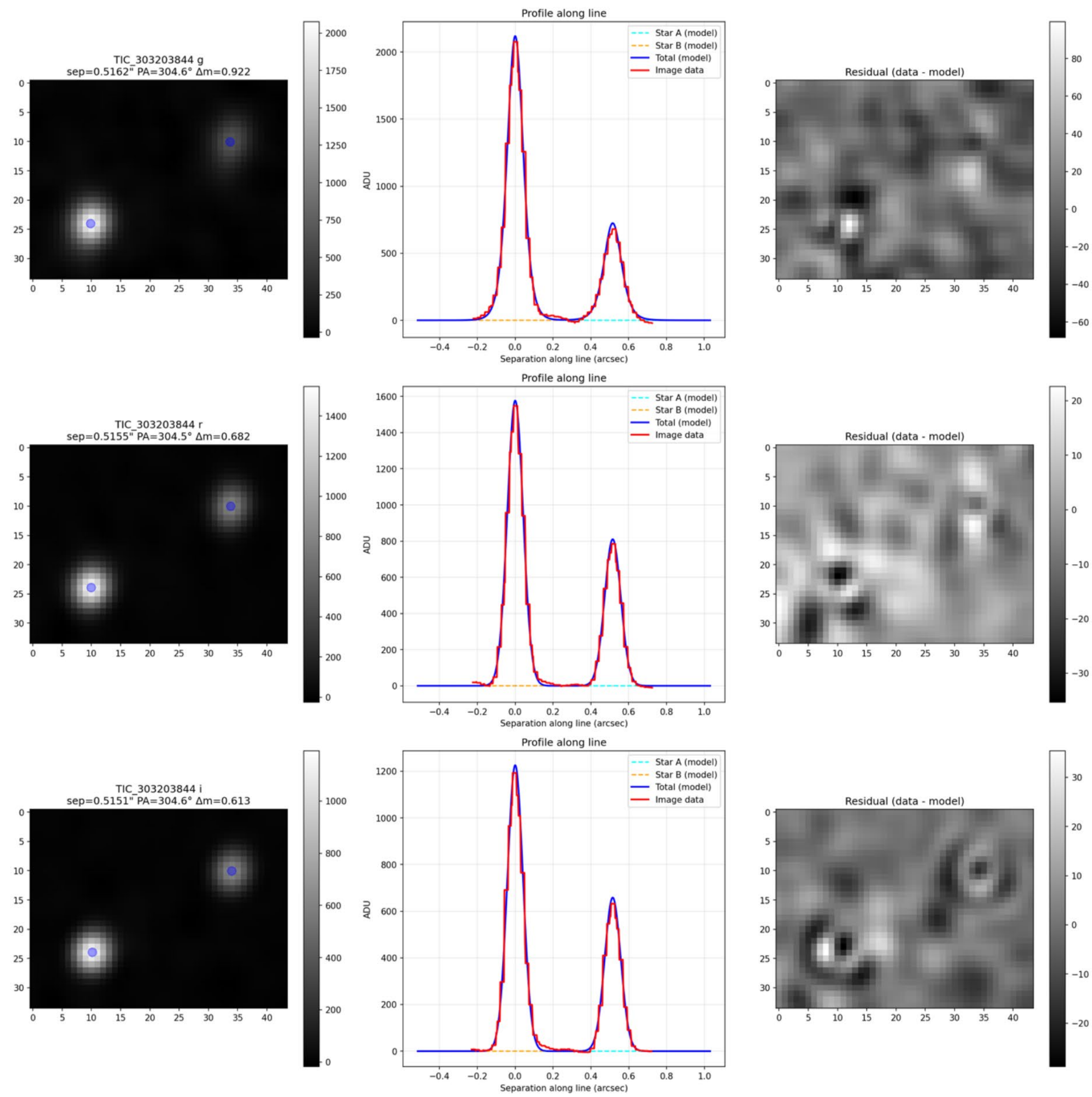

SG04 / TIC_80474910

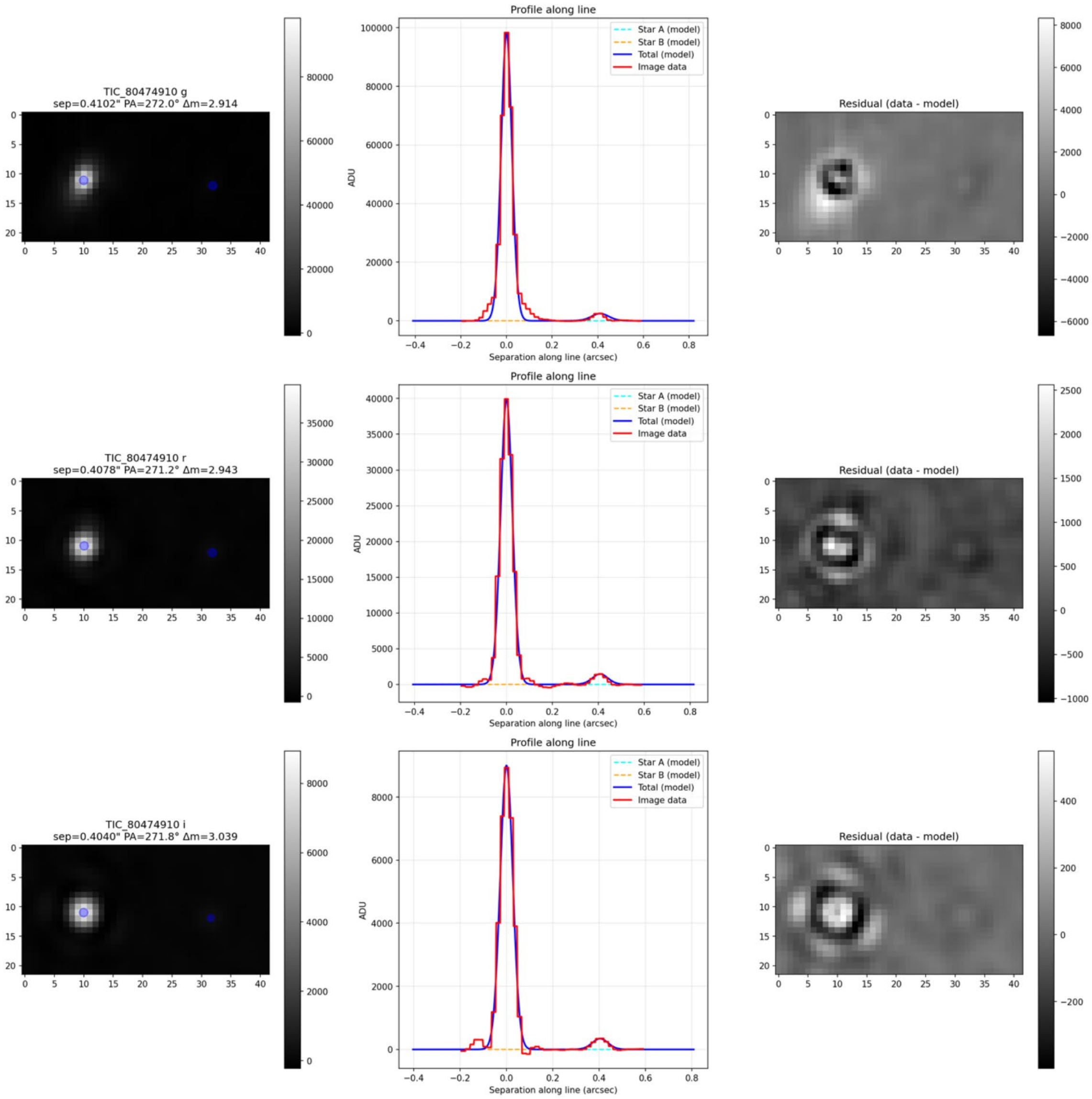

SG118 / TIC_115771549

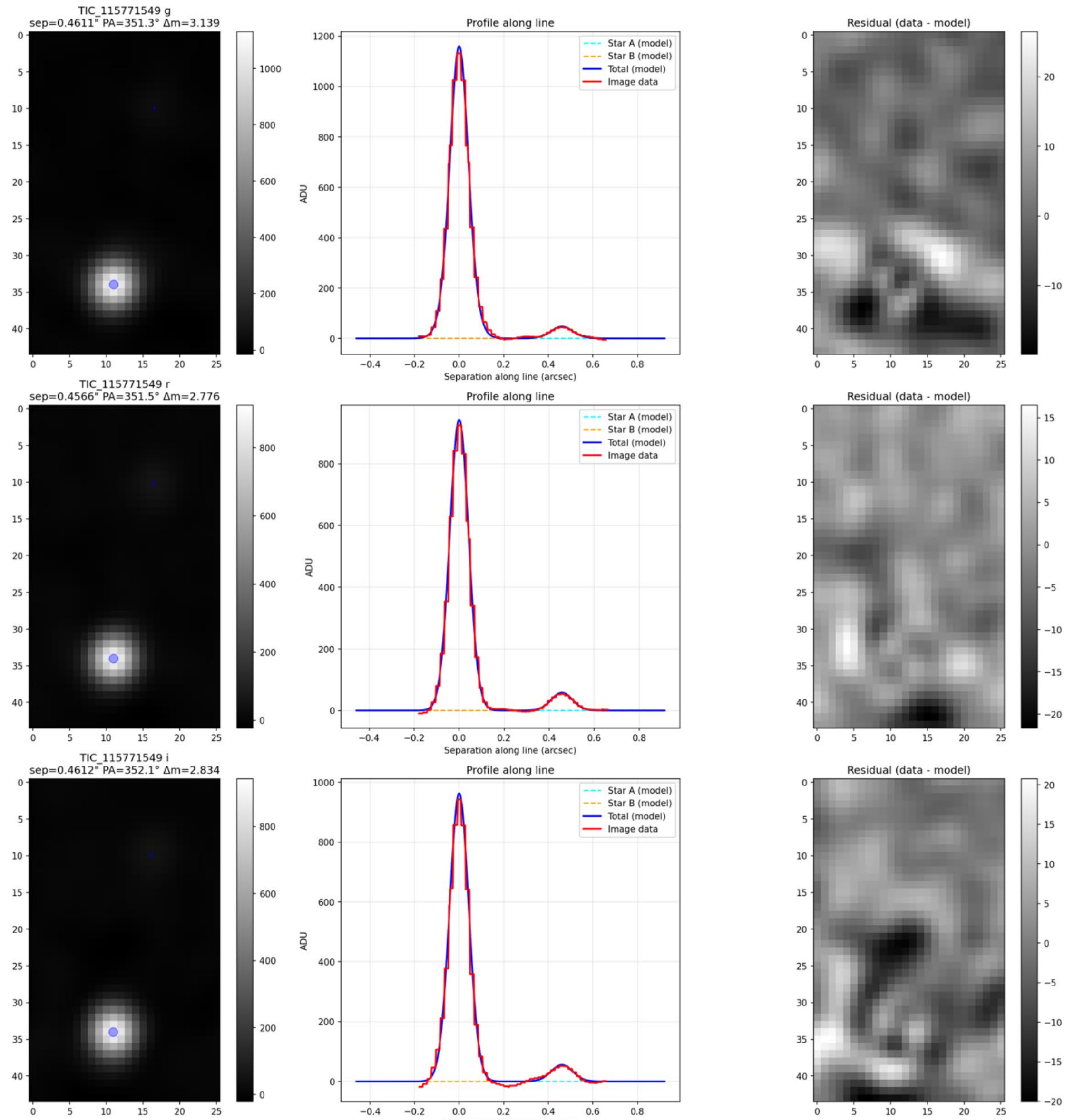

SG119 / TIC_379660147

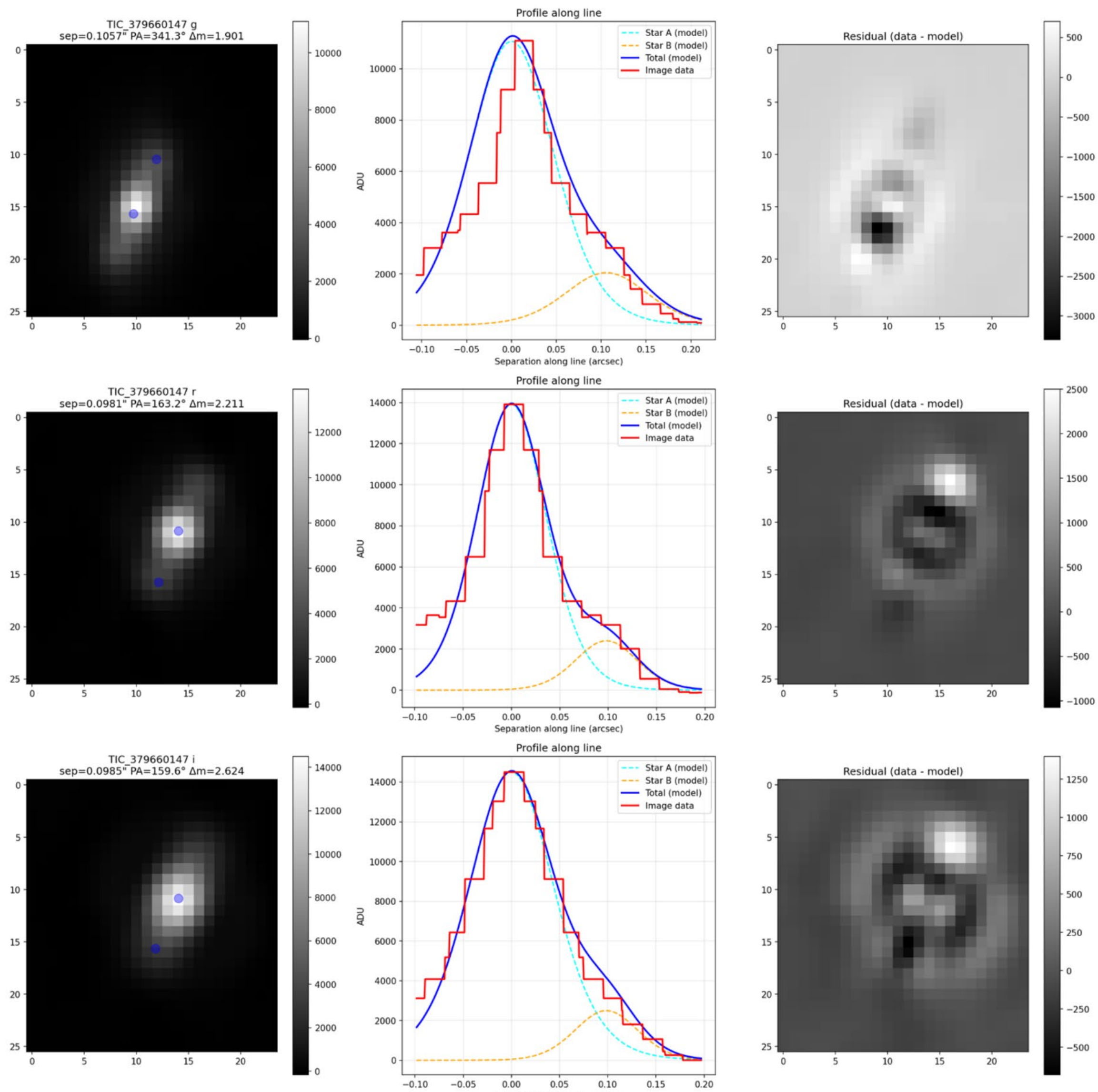

MAT2 / WDS 04201+3108

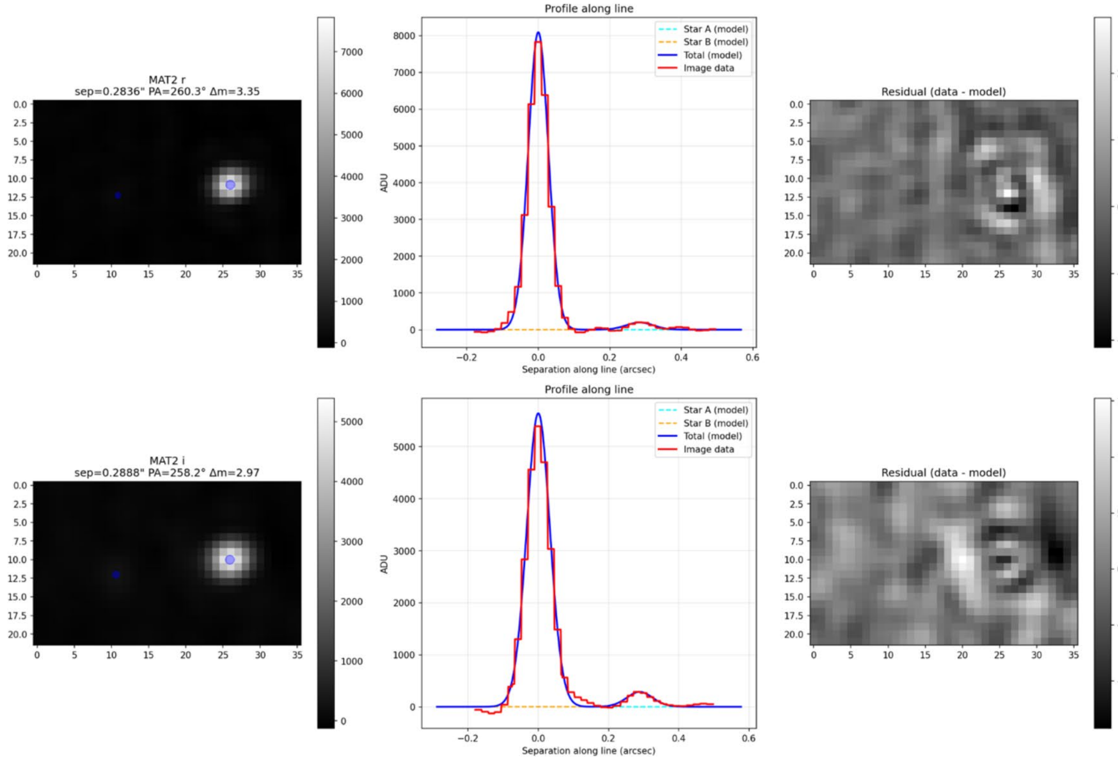

SG11 / TIC_257922326